

Life-cycle based design of mass dampers for the Chilean region and its application for the evaluation of the effectiveness of tuned liquid dampers with floating roof

Rafael Ruiz^{1,2} · Alexandros A. Taflanidis¹ · Diego Lopez-Garcia^{2,3} · Christopher R. Vetter¹

Received: 9 September 2015 / Accepted: 14 December 2015 / Published online: 26 December 2015
© Springer Science+Business Media Dordrecht 2015

Abstract The assessment of the effectiveness of mass dampers for the Chilean region within a multi-objective decision framework utilizing life-cycle performance criteria is considered in this paper. The implementation of this framework focuses here on the evaluation of the potential as a cost-effective protection device of a recently proposed liquid damper, called tuned liquid damper with floating roof (TLD-FR). The TLD-FR maintains the advantages of traditional tuned liquid dampers (TLDs), i.e. low cost, easy tuning, alternative use of water, while establishing a linear and generally more robust/predictable damper behavior (than TLDs) through the introduction of a floating roof. At the same time it suffers (like all other liquid dampers) from the fact that only a portion of the total mass contributes directly to the vibration suppression, reducing its potential effectiveness when compared to traditional tuned mass dampers. A life-cycle design approach is investigated here for assessing the compromise between these two features, i.e. reduced initial cost but also reduced effectiveness (and therefore higher cost from seismic losses), when evaluating the potential for TLD-FRs for the Chilean region. Leveraging the linear behavior of the TLD-FR a simple parameterization of the equations of motion is established, enabling the formulation of a design framework that beyond TLDs-FR is common for other type of linear mass dampers, something that supports a seamless comparison to them. This framework relies on a probabilistic characterization of the uncertainties impacting the seismic performance. Quantification of this performance through time-history analysis is considered and the seismic hazard is described by a stochastic ground motion model that is calibrated to offer hazard-compatibility with ground motion

✉ Alexandros A. Taflanidis
a.taflanidis@nd.edu

¹ Department of Civil and Environmental Engineering and Earth Sciences, University of Notre Dame, Notre Dame, IN 46556, USA

² Department of Structural and Geotechnical Engineering, Pontificia Universidad Católica de Chile, Santiago, Chile

³ National Research Center for Integrated Natural Disaster Management CONICYT/FONDAP/15110017, Santiago, Chile

prediction equations available for Chile. Two different criteria related to life-cycle performance are utilized in the design optimization, in an effort to support a comprehensive comparison between the examined devices. The first one, representing overall direct benefits, is the total life-cycle cost of the system, composed of the upfront device cost and the anticipated seismic losses over the lifetime of the structure. The second criterion, incorporating risk-averse concepts into the decision making, is related to consequences (repair cost) with a specific probability of exceedance over the lifetime of the structure. A multi-objective optimization is established and stochastic simulation is used to estimate all required risk measures. As an illustrative example, the performance of different mass dampers placed on a 21-story building in the Santiago area is examined.

Keywords Mass dampers · Tuned liquid damper with floating roof · Life-cycle performance · Multi-objective design · Chilean seismic risk

1 Introduction

In the last couple of decades the use of supplemental seismic protection devices in Chilean buildings (Zemp et al. 2011; Moroni et al. 2011; De la Llera et al. 2004) has been gaining increased popularity, either as a retrofitting strategy or even for establishing higher performance standards for new structures. One of the devices that have been considered for this purpose (Zemp et al. 2011) is mass dampers (also frequently referenced as inertia dampers). Mass dampers, with most popular representative corresponding to the Tuned Mass Damper (TMD) (Chang 1999; Soto and Adeli 2013), consist of an inertial element (secondary mass) attached to a higher floor of the structure to be controlled (primary mass). Through appropriate tuning of the vibratory characteristics of the inertial element, corresponding to selection of optimal values for its frequency and damping, this secondary mass counteracts the motion of the structure, facilitating the desired energy dissipation for the latter (Den Hartog 1947). Many variations of mass dampers have been proposed in the literature (Chang 1999; Hitchcock et al. 1997; Kareem 1990; Fujino et al. 1992; Balendra et al. 1999; Matta et al. 2009) for improving the dynamic performance of structures under a variety of dynamic excitations. For seismic excitations, though, a reduced effectiveness is generally acknowledged for mass dampers (Soto and Adeli 2013; Lin et al. 2010). This should be attributed to the fact that earthquakes are short-duration, non-stationary excitations, frequently (in near-fault regions) with impulsive characteristics (Mavroeidis et al. 2004; Bray and Rodriguez-Marek 2004). On the other hand, mass dampers, being inertia devices, require typically some rise-time so that their own vibration becomes large enough to facilitate the desired energy dissipation (Lin et al. 2010). This can contribute to potential inefficiency (depending on the characteristics of the excitation) in reducing peak structural responses, which is the main engineering demand parameter of importance when considering seismic performance (Bozorgnia and Bertero 2004; Porter et al. 2007; Vamvatsikos and Cornell 2005). Though mass dampers have been demonstrated very efficient in reducing seismic responses when earthquakes are approximated as stationary excitation (Marano et al. 2007; Taflanidis et al. 2007; Hoang et al. 2008; Daniel and Lavan 2014; Debbarma et al. 2010) or in enhancing the average response even under non-stationary excitations (Wong 2008; Salvi et al. 2014), this efficiency can decrease when performance is evaluated in terms of instantaneous peak quantities (Tributsch and Adam 2012; Lin et al. 2010; Salvi et al. 2014).

A special case of mass dampers are liquid dampers, for which the secondary mass corresponds to a liquid (typically water) inside either a (a) tank (Fujino et al. 1992; Kareem 1990; Tait et al. 2007) or a (b) U-shaped tube (Sakai et al. 1989; Hitchcock et al. 1997; Balendra et al. 1999). Implementation (a) is known as tuned liquid damper or tuned sloshing damper (TLD/TSD) and implementation (b) as liquid column damper, with variants the tuned liquid column damper (TLCD) (Sakai et al. 1989) and the liquid column vibration absorber (LCVA) (Hitchcock et al. 1997). Liquid dampers enjoy some significant advantages such as lower installation costs, easy tuning process for their frequency and potential alternative use of the secondary mass. At the same time they have some potential disadvantages. For liquid column dampers this pertains to their nonlinear internal damping characteristics or the fact that facilitating large masses might impose some architectural challenges for accommodating large tubular sections. For TLDs it pertains to the fact that their dynamic behavior involves nonlinear wave breaking phenomena and that establishing the required optimal level of internal damping requires addition of submerged obstacles (Love and Tait 2010; Kaneko and Mizota 2000) whose behavior is in general difficult to predict. In response to these shortcomings, a new type of TLD was introduced recently (Ruiz et al. 2015b). The new device, also shown in part (a) of Fig. 1, is called tuned liquid damper with floating roof (TLD-FR) and consists of a traditional TLD with the addition of a floating roof. Since the roof is much stiffer than water, it prevents wave breaking, hence making the response linear even at large amplitude of motion. The roof also makes possible the addition of supplemental devices with which the level of damping for the liquid motion can be substantially augmented to match desired optimal values.

Independent of the type of liquid damper, a common characteristic shared by all of them (Chang 1999; Ruiz 2015), and another potential disadvantage, is that only a portion of the total liquid mass contributes in directly controlling the dynamic response of the building. For example for liquid column dampers this is related to the portion of liquid within the horizontal part of the tube whereas for TLDs-FR to the mass participating in the fundamental mode of liquid-vibration, which is related to the tank geometry. This means that for the same total mass, a TMD will offer always greater vibration suppression (Chang 1999; Ruiz 2015). At the same time, though, liquid dampers have smaller installation and maintenance cost (Chang 1999; Love and Tait 2010; Wang et al. 2015; Soto and Adeli

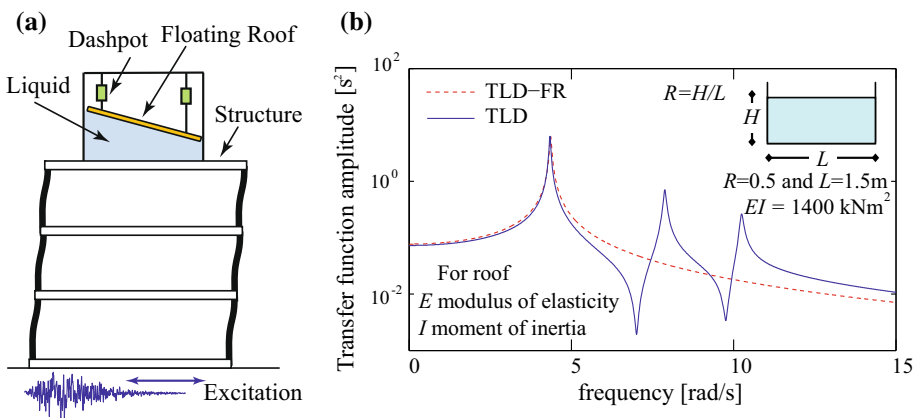


Fig. 1 a Structure equipped with TLD-FR and b transfer function for tuned liquid damper with and without the floating roof for a rectangular tank (characteristics of tank also shown)

2013). Therefore proper comparison of these devices needs to consider the performance over their entire lifetime, incorporating the different level of vibration suppression offered by each but also the different upfront cost characteristics. Though researchers have examined the life-cycle benefits of adding mass dampers (Lee et al. 2012; Tse et al. 2012), no studies exist that have explicitly considered the design based on life-cycle performance criteria, especially examining seismic applications or the comparison of dampers with different upfront cost characteristics. Life-cycle cost based seismic design has been becoming, though, increasingly popular (Ang and Lee 2001; Fragiadakis et al. 2006), especially in the context of evaluation of the effectiveness of supplemental seismic protective devices (Shin and Singh 2014; Gidaris and Taflanidis 2015). This approach considers in the decision making the contributions from the initial (upfront) cost as well as the expected direct and indirect losses due to future seismic events, and therefore has the potential to support a comprehensive assessment of the benefits for different mass damper implementations, providing a socio-economic justification for their adoption.

This paper seeks to address the gaps identified in the previous paragraphs, and sets two goals for a detailed evaluation of the performance of linear mass dampers for the Chilean region: (a) validate the seismic potential considering the characteristics of regional ground motions, and (b) offer a comprehensive life-cycle design/assessment adopting a multi-criteria approach. Goal (b) is the main emphasis on the study, establishing a consistent comparison between TLDs-FR and TMDs considering, as discussed in the previous paragraph, the differences in upfront cost and vibration suppression capabilities. Leveraging the linear behavior of the TLD-FR a simple parameterization of the equations of motion is established enabling the formulation of a common design framework for all types of linear mass dampers. Life-cycle performance is quantified through the probabilistic framework developed by Taflanidis and Beck (2009) with the seismic hazard represented through a stochastic ground motion model that is calibrated here to offer hazard-compatibility to ground motion prediction equations (attenuation relationships) available for Chile (Boroschek and Contreras 2012). Two different criteria related to life-cycle performance are utilized in an effort to support a comprehensive comparison between the examined devices. The first one, representing overall direct benefits, is the total life-cycle cost of the system, composed of the upfront device cost and the anticipated seismic losses over the lifetime of the structure. The second criterion, incorporating risk-averse concepts into the decision making (Cha and Ellingwood 2012; Gidaris et al. 2014), is related to consequences (repair cost) with a specific probability of exceedance over the lifetime of the structure. A multi-objective optimization is therefore established, facilitating a detailed evaluation of the upfront damper cost on the established performance, and therefore the intended comparison between different mass dampers.

In the next section, the potential efficiency of mass dampers for the Chilean region is examined and the appropriateness of the stochastic ground motion model that will be used for the life-cycle assessment is evaluated. Then Sect. 3 briefly reviews the numerical modelling for the TLD-FR. In Sect. 4 the multi-objective design theoretical framework and its computational implementation are discussed and in Sect. 5 the hazard-compatible ground motion model for Chile is developed. Finally, Sect. 6 presents the case study, considering an existing building in the Santiago area, and provides answers for the seismic potential of TLDs-FR as a protection device for Chilean buildings. Within this case study, the impact of structural uncertainties on the design and associated performance is also examined, an issue of acknowledged importance for mass dampers (Chakraborty and Roy 2011; Debbarma et al. 2010).

2 Effectiveness of mass dampers for suppressing vibrations for earthquakes in the Chilean region

As it was mentioned in the introduction, the effectiveness of mass dampers in controlling transient seismic vibrations depends upon the characteristics of the excitation; the correct tuning of the mass damper properties is mandatory but not sufficient to guarantee a good performance. Considering this challenge the potential of mass dampers for seismic applications for Chilean buildings is verified in this section. A particular assumption here is that the mass of the mass damper is only a small percentage of the mass of the primary structure. Though high efficiency in consistently suppressing seismic vibrations (i.e., independently of the characteristics of the excitation) has been reported when large masses are adopted (Matta 2011; De Angelis et al. 2012) and innovative approaches have been developed to accommodate the addition of such large masses (Matta and De Stefano 2009) or create an equivalent effect though incorporation of a passive inerter (Marian and Giaralis 2014), for the applications examined here (emphasis on TLD-FR) such an adoption should be considered as impractical.

The effectiveness of mass dampers for Chilean buildings is directly related to the seismicity of the region and the characteristics of typical earthquake ground motions. This seismicity is associated with the subduction zones at the Chilean coast which result in strong and long-duration excitations (Leyton et al. 2009), with far-field characteristics: (a) rupture distances for major events greater than 30 km for most important cities (Boroschek and Contreras 2012), (b) ground motion records that lack pulse-like waveforms in the velocity time histories and (c) large durations. These characteristics indicate that the implementation of mass dampers to control the seismic response of Chilean buildings has the potential to provide substantial benefits. This is further validated by examining the performance of the structure that will be considered in the case study later (Sect. 6) equipped with a TMD with mass equal to 1 % of the total mass of the building and optimally designed for stationary base-excitation. Three different sets of ground motion are considered in the comparison. The first set, denoted as *Chilean records*, corresponds to 11 typical Chilean ground motions taken from the RENADIC (National Accelerograph Network at the Department of Civil Engineering, Universidad de Chile) database, associated with different important seismic events in Chile the past 30 years. The second set, denoted

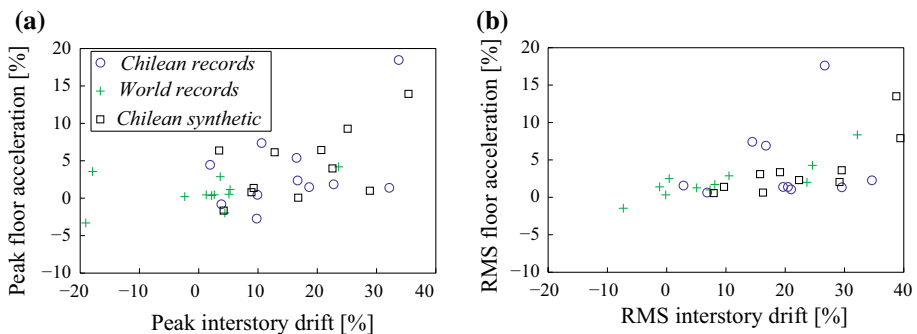


Fig. 2 Mass damper efficiency (response reduction) for inter-story drift and floor acceleration (maxima over all floors reported) for three sets of ground motions (*scatter plots*) for **a** peak response and **b** RMS response

as *World records*, corresponds to an additional 11 ground motions, most of them from the US West coast and many of them including a pulse-like components (seismic events at near-fault region). Details about both these sets are provided in (Ruiz 2015). The third, and final, set of ground motions, denoted as *Chilean synthetic*, are obtained employing the stochastic ground motion modeling procedure that will be described in Chapter 6 that provides excitations compatible with the Chilean seismic hazard. The characteristics of these motions (moment magnitude and rupture distance) mirror the one from the first set. Seismic performance is evaluated using inter-story drifts and floor acceleration (maximum responses over all floors are used) and both these quantities are evaluated either as instantaneous peak responses or average RMS (root mean square) responses. The percentage reduction through the introduction of the damper is used to quantify the damper-efficiency and results are presented in Fig. 2. Note that positive values for this reduction correspond to benefit from the addition of the damper.

Comparing the first two sets of motion, it is evident that for peak drift-responses significant reduction is established for *Chilean records* over all examined ground motions, with values as high as 30 %, whereas for *World records* minimal improvement is overall reported (or even amplification of the response for some instances). When looking at RMS responses the benefit from the mass damper implementation is significantly improved, especially for *World records*. This validates the arguments made above; earthquakes that are typical in Chilean region accommodate the reduction of peak seismic responses (not just RMS responses) through inertia devices. Note that this improvement is relatively smaller for the peak acceleration responses when compared to the peak drift responses. This should be attributed to fact that the acceleration responses are impacted by higher modes which the TMD cannot control. This feature has on its own important implications: even for excitations for which TMDs can provide improvement of structural responses, this improvement is expected larger for drift demands rather than acceleration demands. Comparing further the first and third sets of motion shows that the trends for the actual (*Chilean records*) and the synthetic motions (*Chilean synthetic*) are similar, demonstrating that the synthetic motions provided by the ground motion modeling scheme developed in Sect. 5 establish a similar behavior for a structure equipped with mass dampers as the response obtained from regional earthquakes. This is an important feature, showing that the developed ground motion model should be considered to be able to describe adequately the seismic hazard for the application examined in this paper.

3 Equations of motion for a structure with a TLD-FR and relationship to other type of mass dampers

This section reviews the equation of motion for a TLD-FR and established a unified representation for all type of linear mass dampers to support the intended seamless comparison between them. Formulation here assumes a planar structural model, though mass dampers (especially TLDs-FR) can be potentially considered for bi-directional control applications.

3.1 Equation of motion for TLD-FR

The schematic of the TLD-FR is shown in Fig. 1a. Its dynamic characteristics depend on the tank geometry, the roof stiffness, the height of the liquid within the tank as well as the

characteristics of the external dampers. The numerical model for the TLD-FR is presented in detail in (Ruiz et al. 2015b). Experimental validation of this model has shown (Ruiz et al. 2015b) that the introduction of the roof of the TLD-FR prevents wave breaking phenomena, resulting in a practically linear response even at larger amplitudes. Additionally, the roof helps suppress higher modes of vibration while having negligible impact on the fundamental mode, as also shown in Fig. 1b; in that plot TLD and TLD-FR have identical response for 1st mode but higher modes are suppressed for the TLD-FR. Taking advantage of the linear characteristics of the response and through modal analysis and proper truncation (retaining only the first, dominant mode, which is also the mode tuned to the structure), the dynamic behaviour of the TLD-FR can be approximated though a single degree of freedom model as shown in detail in (Ruiz et al. 2015b). A key point related to this behaviour is that only a portion of the liquid mass participates in the sloshing in this mode, something that ultimately reduces the efficiency of the device. This may be equivalently interpreted by distinguishing the total mass to two different components (Housner 1957): one that is rigidly attached to the tank walls (impulsive mass) and another one attached by a spring and a damper (convective mass).

A simplified parameterization of the equation of motion of the TLD-FR can be further established (Ruiz et al. 2015b) through only four parameters: three of them are the traditional parameters used to describe linear mass dampers, the total liquid mass m (or more general mass of the damper), the natural frequency ω_m and the damping ratio ξ_m , while the fourth parameter is called efficiency index γ and is related to the amount of liquid that participates in the sloshing in the fundamental mode. All these parameters can be related to the tank geometry and damper properties (Ruiz et al. 2015b). A review of this parametric formulation along with basic details for the equations of motion for the TLD-FR is offered in Appendix A. Herein the parametric formulation will be utilized for describing the TLD-FR, understanding that these parameters depend ultimately on the tank geometry characteristics, with the latter readily identified once an appropriate parametric description is chosen.

Through this modal truncation and parameterization the equation of motion for the TLD-FR can be finally described as (Ruiz et al. 2015b):

$$\ddot{y}_n + 2\xi_m \omega_m \dot{y}_n + \omega_m^2 y_n = -\ddot{u}_b \quad (1)$$

where \ddot{u}_b corresponds to the acceleration at the base of the TLD-FR and y_n represents a modal quantity related to the response of the floating roof. This can be viewed ultimately as an equivalent generalized displacement for the roof [full details for the definition are included in (Ruiz et al. 2015b)]. The transmitted force F at the base of the TLD-FR, used to couple its behavior to the vibration of the structure it is placed upon, is given by (Ruiz et al. 2015b):

$$F/m = -\gamma \ddot{y}_n - \ddot{u}_b \quad (2)$$

This transmitted force exhibits a dependence on the efficiency index. An efficiency index equal to unity indicates that the whole liquid mass has a dynamic effect on the transmitted force; this is identical to the traditional case for the TMD (Chang 1999), described through (1) and (2) but with $\gamma = 1$ and y_n corresponding to the relative response of the secondary mass. This set of equations is also identical to the one that can be derived to describe the behavior of liquid column dampers (TLCDs/LCVAs) (Taflanidis et al. 2007), in this case with the efficiency index related to the percentage of the total mass that

participates in the liquid vibration in the horizontal direction (horizontal part of the tube) and y_n related to the displacement of the liquid column.

Therefore, through the introduction of the efficiency index γ a common characterization of three different mass dampers is accomplished through Eqs. (1) and (2) with the TMD corresponding to $\gamma = 1$. For the same mass m larger values of efficiency index correspond always to higher performance for properly designed (i.e. tuned) mass dampers (Taflanidis et al. 2007; Chang 1999; Ruiz 2015), in other words the TMD will always outperform liquid dampers of the same mass. Should be also stressed that TLDs-FR can be easily configured to provide larger values of γ [as high as 0.6–0.8] (Ruiz 2015) something that is challenging for liquid-column dampers [values close to 0.4–0.6 are more reasonable for their implementation]. Herein the discussion will focus on TLDs-FR, with the understanding, though, that through the representation by Eqs. (1) and (2) all aforementioned mass dampers are simultaneously covered.

3.2 Equation of motion for structure with a TLD-FR (mass damper)

Consider now an n -degree of freedom structure with a TLD-FR, located in a particular floor described through the location vector $\mathbf{L} \in \mathfrak{R}^{1 \times n}$ (row vector of zeros with a single 1, at the floor of the TLD-FR). Linear structural behavior is assumed here since it has been shown that for the Chilean region modern design/construction practices results in structures that demonstrate practically linear behavior even under strong excitations (EERI Special Earthquake Report 2010). Let $\mathbf{u} \in \mathfrak{R}^{n \times 1}$ denote to the vector of displacements (relative to the ground) of each floor, $\mathbf{R} \in \mathfrak{R}^{n \times 1}$ the vector of earthquake influence coefficients and \mathbf{M}_s , \mathbf{C}_s and \mathbf{K}_s the $\mathfrak{R}^{n \times n}$ mass, damping and stiffness matrices, respectively. Using (2) for the force transmitted from the TLD-FR to the structure while expressing as $\ddot{u}_b = \mathbf{L}(\ddot{\mathbf{u}} + \mathbf{R}\ddot{u}_g)$ the acceleration at the base of the TLD-FR in both (1) and (2) the system of equations of motion for the structure equipped with the TLD-FR (or general mass damper) is (Taflanidis et al. 2007)

$$\begin{aligned} & \begin{bmatrix} \mathbf{M} + \mathbf{L}^T m \mathbf{L} & \mathbf{L}^T m \gamma \\ \mathbf{L} & 1 \end{bmatrix} \begin{bmatrix} \ddot{\mathbf{u}} \\ \ddot{y}_n \end{bmatrix} + \begin{bmatrix} \mathbf{C} & 0 \\ \mathbf{0} & 2\xi_m \omega_m \end{bmatrix} \begin{bmatrix} \dot{\mathbf{u}} \\ \dot{y}_n \end{bmatrix} + \begin{bmatrix} \mathbf{K} & 0 \\ \mathbf{0} & \omega_m^2 \end{bmatrix} \begin{bmatrix} \mathbf{u} \\ y_n \end{bmatrix} \\ & = - \begin{bmatrix} (\mathbf{M} + \mathbf{L}^T m \mathbf{L}) \mathbf{R} \\ \mathbf{L} \mathbf{R} \end{bmatrix} \ddot{u}_g \end{aligned} \tag{3}$$

A dimensional characterization may be then established by using $m = r \cdot m_t$ and $\omega_m = \alpha \cdot \omega_1$, where m_t is the total structural mass and ω_1 the fundamental structural frequency. The variables r and α represent the mass and frequency ratios, respectively.

4 Multi-criteria design based on life-cycle performance metrics

4.1 Probabilistic characterization of life-cycle performance

Quantification of seismic risk and through that of the life-cycle performance is established through the framework discussed in (Taflanidis and Beck 2009). The framework, shown in Fig. 3, is based on adoption of appropriate models for the seismic excitation (hazard analysis), structural system (structural analysis) and loss evaluation (damage and loss analysis), and on assigning appropriate probability distributions to the parameters that are

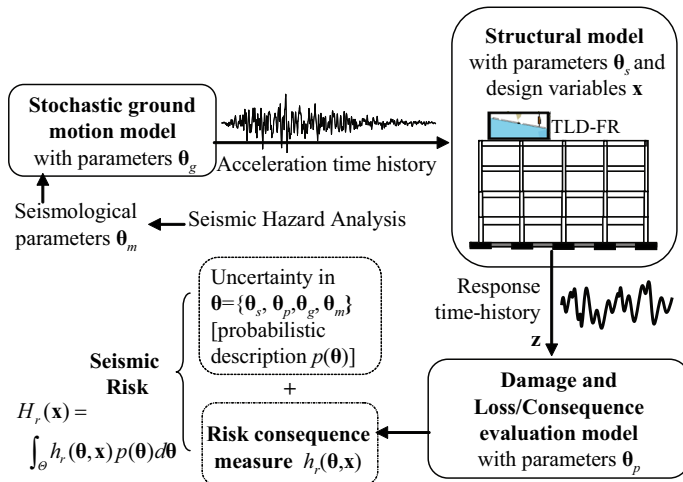


Fig. 3 Schematic for risk quantification framework

considered as uncertain in these different models. The latter uncertainty characterization supports ultimately the seismic risk quantification. Structural behavior is evaluated through time-history analysis and seismic consequences through an assembly-based vulnerability approach (Porter et al. 2001), whereas for providing an appropriate within this context description of the seismic excitation (acceleration time-histories) a stochastic ground motion modeling approach is utilized, established by modulating a high-dimensional white noise sequence through functions that address the frequency and time-domain characteristics of the excitation. The ground motion model involves as inputs seismological characteristics, the moment magnitude M and the rupture distance r_{rup} , and can be tuned, as will be discussed in Sect. 5, to provide a hazard compatibility by establishing a match to regional ground motion prediction equations. Adoption of probability distributions for the seismological parameters facilitates then a comprehensive probabilistic description of the seismic hazard (Jalayer and Beck 2008).

In this context, let θ lying in $\Theta \subset \mathbb{R}^{n_\theta}$ denote the augmented vector of continuous uncertain model parameters with probability density functions (PDFs) denoted as $p(\theta)$, where Θ denotes the space of possible parameter-values. This vector includes all the different parameters (either seismological, or structural) that are considered as uncertain as well as the white noise sequence utilized in the ground motion model. Also, let the vector of controllable parameters for the mass damper referred to herein as *design variables*, be $\mathbf{x} \in X \subset \mathbb{R}^{n_x}$, where X denotes the admissible design space. Ultimately \mathbf{x} includes the mass m (or mass ratio ρ), the natural frequency ω_m (or frequency ratio α), the efficiency index γ and the damping ratio ζ_m . For a specific design configuration \mathbf{x} the risk consequence measure, describing the favorability of the response from a decision-theoretic point of view, is given by $h_r(\theta, \mathbf{x})$. Each consequence measure $h_r(\cdot)$ is related to (1) the earthquake performance/losses that can be calculated based on the estimated response of the structure \mathbf{z} (performance given that some seismic event has occurred), as well as to (2) assumptions made about the rate of occurrence of earthquakes (incorporation of the probability of seismic events occurring). Seismic risk, $H_r(\mathbf{x})$, is then described through the expected value of the risk-consequence measure, given by the generic multi-dimensional integral

$$H_r(\mathbf{x}) = \int_{\Theta} h_r(\boldsymbol{\theta}, \mathbf{x}) p(\boldsymbol{\theta}) d\boldsymbol{\theta} \quad (4)$$

Through different selection of the risk consequence measure different risk quantifications can be addressed within this framework, supporting the estimation of all necessary life-cycle performance metrics.

4.2 Life-cycle performance design metrics

The main metric utilized in the design formulation is the total life-cycle cost $C(\mathbf{x}) = C_i(\mathbf{x}) + C_l(\mathbf{x})$, provided by adding the initial (upfront) cost $C_i(\mathbf{x})$, which is a function of the dimensions of the mass damper (mainly its total mass), and the cost due to earthquake losses over the life-cycle of the structure $C_l(\mathbf{x})$. For a Poisson assumption for occurrence of earthquakes (i.e., independent occurrence of seismic events), as considered in the example later, the present value $C_l(\mathbf{x})$ of expected future seismic losses is given by integral (4) with associated risk consequence measure definition (Goulet et al. 2007)

$$h_r(\boldsymbol{\theta}, \mathbf{x}) = C_r(\boldsymbol{\theta}, \mathbf{x}) v t_{life} \left[\frac{1 - e^{-r_d t_{life}}}{r_d t_{life}} \right] \quad (5)$$

where r_d is the discount rate, t_{life} is the life cycle considered and $C_r(\boldsymbol{\theta}, \mathbf{x})$ is the cost given the occurrence of an earthquake event. For estimating the latter an assembly-based vulnerability approach is adopted as discussed earlier. According to this approach the components of the structure are grouped into damageable assemblies, which consist of components of the system that have common vulnerability and repair cost characteristics (e.g. ceiling, wall partitions, etc.). Different damage states are designated to each assembly and a fragility function (quantifying the probability that a component has reached or exceeded its damage state) and repair cost estimates are established for each damage state. The former is conditional on some engineering demand parameter (*EDP*), which is related to peak characteristics for the structural response (e.g. peak interstory drift, peak floor acceleration, etc.). Combination of the fragility and cost information provides then $C_r(\boldsymbol{\theta}, \mathbf{x})$.

Consideration of only the life-cycle cost as performance objective facilitates what is commonly referenced as “*risk-neutral*” design, which assumes that preference is assessed only through quantities that can be monetized. Frequently nontechnical factors, such as social risk perceptions, need to be taken into account that lead to more conservative designs (*risk aversion*), since *risk-neutral* design does not explicitly address the unlikely but potentially devastating losses that lie on the tail of the losses/consequence distribution (Cha and Ellingwood 2012). Motivated by this realization the incorporation of an additional performance objective corresponding to repair cost with specific probability of exceedance over the life-cycle of the structure was suggested in Gidaris et al. (2014). This approach is adopted here. Based on the Poisson assumption of seismic events, the probability of the repair costs C_r exceeding a targeted threshold $C_{thresh}(\mathbf{x})$ over the considered lifetime of the structure is

$$P[C_r > C_{thresh}(\mathbf{x}) | \mathbf{x}, t_{life}] = 1 - \exp^{-t_{life} v \cdot P[C_r > C_{thresh}(\mathbf{x}) | \mathbf{x}, \text{event}]} \quad (6)$$

where $P[C_r > C_{thresh}(\mathbf{x}) | \mathbf{x}, \text{event}]$ is the probability of exceeding the repair threshold given that a seismic event has occurred, which is given by the generic risk integral (4) with risk consequence measure

$$h_r(\boldsymbol{\theta}, \mathbf{x}) = I_C(\boldsymbol{\theta}, \mathbf{x}) \tag{7}$$

corresponding to an indicator function, being one if $C_r(\boldsymbol{\theta}, \mathbf{x}) > C_{thresh}(\mathbf{x})$ and zero if not.

4.3 Multi-objective design problem

The multi-criteria design is expressed ultimately as

$$\begin{aligned} \mathbf{x}^* = \arg \min_{\mathbf{x} \in X} \{ & C(\mathbf{x}) = C_i(\mathbf{x}) + C_l(\mathbf{x}), C_{thresh}(\mathbf{x}) \}^T \\ \text{such that } & P[C_r > C_{thresh}(\mathbf{x}) | \mathbf{x}, t_{life}] = p_o \end{aligned} \tag{8}$$

where $C(\mathbf{x})$ [first objective] is the life-cycle cost and $C_{thresh}(\mathbf{x})$ [second objective] is the repair threshold with probability of being exceeded p_o over the lifetime of the structure. This multi-objective formulation leads ultimately to a set of points (also known as dominant designs) that lie on the boundary of the feasible objective space and they form a manifold, which is called Pareto front. A point belongs to the Pareto front and it is called Pareto optimal point if there is no other point that improves one objective without detriment to the other. The motivation behind the multi-objective formulation of the problem is that the decision-maker (e.g. building owner) can choose among a range of TLD-FR configurations (Pareto optimal solutions) that describe different decision making attitudes towards risk.

4.4 Computational approach for the multi-objective design problem

Optimization (8) requires different risk metrics, $C(\mathbf{x})$ and $C_{thresh}(\mathbf{x})$, whose estimation involves calculation of a probabilistic integral of the form (4). Stochastic simulation is adopted here for this estimation: using a finite number, N , of samples of $\boldsymbol{\theta}$ drawn from proposal density $q(\boldsymbol{\theta})$, an estimate for the risk integral of interest [expressed through generalized form of (4)] is:

$$\hat{H}_r(\mathbf{x}) = \frac{1}{N} \sum_{j=1}^N h_r(\mathbf{x}, \boldsymbol{\theta}^j) \frac{p(\boldsymbol{\theta}^j)}{q(\boldsymbol{\theta}^j)} \tag{9}$$

where $\boldsymbol{\theta}^j$ denotes the sample used in the j th simulation and $\{\boldsymbol{\theta}^j; j = 1, \dots, N\}$ represents the entire sample-set. The proposal density $q(\boldsymbol{\theta})$ is used to improve the efficiency of this estimation [reduce the coefficient of variation of that estimate], by focusing the computational effort on regions of the Θ space that contribute more to the integrand of the probabilistic integral in (4)-this corresponds to the concept of importance sampling (IS). To avoid numerical problems use of IS densities should be utilized only for the considered as probabilistically important model parameters and use $q(\cdot) = p(\cdot)$ for the rest. Further details on selection of such IS densities for seismic applications can be found in Taflanidis and Beck (2009).

The design problem in (8) is ultimately solved by substituting the stochastic simulation estimates of form (9) for the required probabilistic integrals. The existence of the prediction error (stemming from the stochastic simulation) within the optimization (resulting in a so-called stochastic optimization problem) is addresses by adopting an exterior sampling approach (Spall 2003), utilizing the same, sufficiently large, number of samples throughout all iterations in the optimization process, i.e. $\{\boldsymbol{\theta}^j; j = 1, \dots, N\}$ for (9) is chosen the same for each design configuration examined, therefore reducing the importance of the

estimation error in the comparison of different design choices (creating a consistent error in these comparisons).

Furthermore, for supporting an efficient optimization an approach relying on kriging surrogate modeling is adopted following the guidelines discussed in Gidaris and Taflanidis (2015). The surrogate model is established here to provide an approximate relationship between the design selection \mathbf{x} (input to the surrogate model) and the risk quantities needed in the optimization (8), $C_{thresh}(\mathbf{x})$ and $C_l(\mathbf{x})$ (outputs for the surrogate model) and is developed through the following approach. A large set of design configurations (1000 in the case study discussed later) for the TLD-FR is first established to serve as support points for the kriging, utilizing a latin hypercube sampling in X . The response of each design configuration is then evaluated through time-history analysis, and then the risk quantities C_l and C_{thresh} are calculated. Using this information the kriging metamodel is developed. This metamodel allows a highly efficient estimation of the risk measures of interest (thousands of evaluations within minutes) and is then used within the multi-objective optimization (8), coupled with an appropriate assumption for the upfront damper cost (used to calculate the overall cost C). Note that the metamodel is independent of the upfront damper cost assumptions so needs to be built only once for all the cases considered with respect to the latter. The multi-objective problem can be then solved through any appropriate method, for example through a blind-search approach or through the implementation of a genetic algorithm (Coello et al. 2002; Marler and Arora 2004).

5 Hazard-compatible ground motion modeling for Chile

Seismic hazard in the proposed framework (Fig. 3) needs to be described in terms of acceleration time-histories. As discussed in Sect. 4.1, a stochastic ground motion modeling approach is utilized here for this purpose. In particular a site-based modeling approach is adopted (Papadimitriou 1990; Rezaeian and Der Kiureghian 2010). The essential component of this approach is the development of the predictive relationship between the parameters of the model (θ_g in Fig. 3), representing characteristics such as the duration of excitation or Arias intensity, and the seismological parameters (θ_m in Fig. 3), such as moment magnitude, M , and rupture distance, r_{rup} . These predictive relationships are ultimately established by considering site-specific characteristics of the seismic hazard and regional recorded ground motions. This is formulated as optimization problem where the coefficients in the predictive relationships (connecting θ_g to θ_m) are identified to provide the desired match.

Here, the framework from (Vetter et al. 2015) is adopted for this optimization, with site-specific compatibility provided through regional ground motion predictive equations (GMPEs), an approach for tuning of ground motion models initially presented in Scherbaum et al. (2006). Such GMPEs (frequently also referenced as attenuation relationships) provide estimates of the peak ground and spectral acceleration as a function of θ_m and represent the established approach for developing seismic hazard maps (Power et al. 2008). Therefore compatibility of the response predictions provided by ground motion models to such GMPEs is facilitating a hazard-compatible description. The framework in Vetter et al. (2015) supports a computationally efficient tuning of any stochastic ground motion model to match the GMPE estimates for a specific structure (defined through the structural periods of interest) and a specific seismicity range (defined by selected value ranges for M and r_{rup}). In this approach, the objective function for the predictive relationship

optimization corresponds to the discrepancy between the GMPE and the mean predictions of the synthetic excitations provided through the stochastic ground motion model. In addition, the optimization problem incorporates as constraints (Vetter et al. 2015) the requirement that the resulting predictive relationships follow regional observed trends for the relationship between θ_m and θ_g . This is an essential component of the approach so that the resultant ground motions have realistic characteristics.

Following this methodology, a versatile stochastic ground motion model based on the suggestions by Papadimitriou (1990) is tuned to match the GMPE presented recently for Chile in (Boroschek and Contreras 2012). This model addresses both temporal and spectral non-stationarities. The former is established through a time-domain modulating envelope function while the latter is achieved by filtering a white-noise process by a filter corresponding to multiple cascading SDOF oscillators with time-varying characteristics. A quick review of the model is offered in the Appendix B, including the functional form of the predictive relationships adopted as well as the optimized coefficients obtained. Results from this hazard compatibility are presented in Fig. 4 for the case study that is examined in the next Section. The intended match of the stochastic ground motion predictions to the

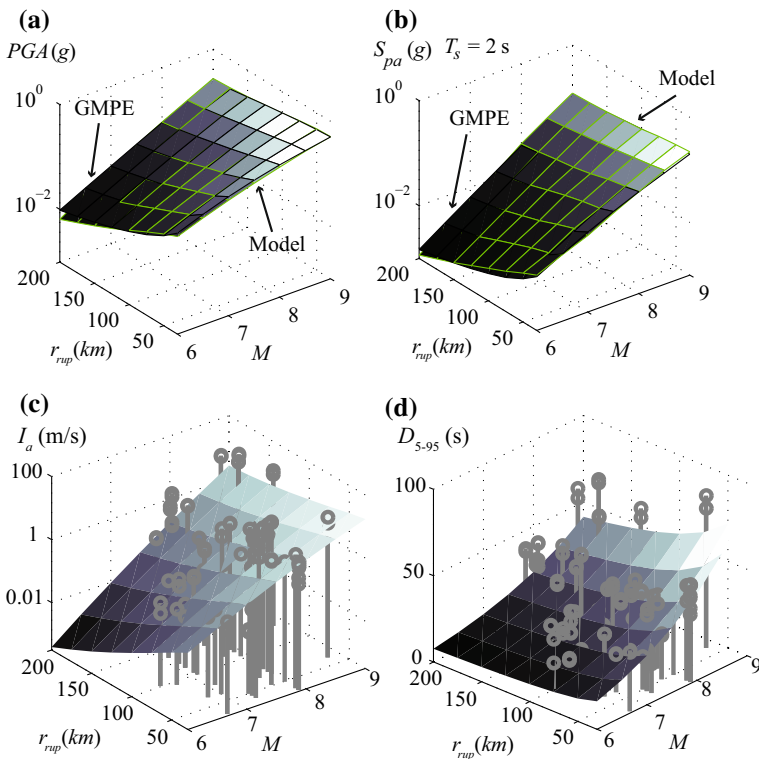


Fig. 4 Results for hazard compatible ground motion modeling for a range of different M - r_{rup} values. *Top row* (parts **a** and **b**) show comparison between GMPE and mean responses of the ground motion model for peak ground acceleration PGA (part **a**) and peak spectral acceleration S_{pa} for 5 % damped elastic SDOF with period $T_s = 2$ s (part **b**). *Bottom row* (parts **c** and **d**) shows the resultant predictive equations for Arias intensity I_a (part **c**) and significant duration D_{s-95} (part **d**) as surface plots as well as samples from regional (recorded) ground motions

desired GMPE is established for the peak ground acceleration (*PGA*) and the peak spectral acceleration S_{pa} for 5 % damped elastic SDOFs with period T_s 2 s, chosen close to the fundamental period of the structure of interest, and for M and r_{rup} in the ranges anticipated to contribute to the seismic risk in this case study. Top row of Fig. 4 [parts (a) and (b)] shows the match of the mean responses of the ground motion model to the GMPE and bottom row [parts (c) and (d)] compares the predictive relationship for two of the model parameters (Arias intensity and significant duration) against available samples from regional ground motions. A very good match to the GMPE is reported, whereas the predictive relationships show very good compatibility with observed regional trends. Furthermore, the comparison between the synthetic ground motions obtained from the optimized ground motion model and regional earthquakes demonstrate, similarly, a good match when examining the response of a structure with a mass damper in Fig. 2 earlier, (compare the *Chilean records* and *Chilean synthetic* sets there). These overall comparisons show that the adopted ground motion modeling approach provides a hazard description that should be considered appropriate for the life-cycle performance assessment for mass dampers in the Chilean region.

6 Case study

As case study the design of a TLD-FR for a 21-story structure located in Santiago is considered. The building corresponds to an existing structure (Zemp et al. 2011) with tapered elliptical shape, length 76.2 m and average depth 20 m (this dimension varies across the length), and has already a TMD installed in its last floor across its slender axis. Same implementation is examined here. Next the numerical and probability models adopted for the seismic hazard and the structure are reviewed, and then results for different assumptions for the upfront cost, ranging from typical values for TMDs to anticipated cost for TLDs-FR, are discussed in detail.

6.1 Seismic hazard model

Seismic events are assumed to occur following a Poisson distribution and so are independent of previous occurrences. The uncertainty in moment magnitude M is modeled by the Gutenberg-Richter relationship truncated on the interval $[M_{min}, M_{max}] = [5.5, 9.0]$, (events smaller than M_{min} do not contribute to the seismic risk) which leads to $p(M) = b_M e^{-b_M M} / (e^{-b_M M_{min}} - e^{-b_M M_{max}})$ and expected number of events per year $v = e^{a_M - b_M M_{min}} - e^{a_M - b_M M_{max}}$. The regional seismicity factors b_M and a_M are chosen by averaging the values for the seismic zones close to Santiago based on the recommendations in (Leyton et al. 2009). This results to $b_M = 0.8 \log_e(10)$ and $a_M = 5.65 \log_e(10)$. Regarding the uncertainty in the event location, the closest distance to the fault rupture, r_{rup} , for earthquake events is assumed to follow a beta distribution in [30 250] km with median $r_{med} = 100$ km and coefficient of variation 35 %. Time-histories are obtained through the model discussed in Sect. 5. This seismic hazard characterization (probability model for M and r_{rup} along with the adopted stochastic ground motion model) results in peak ground acceleration (PGA) with probability of exceedance 10 % in 50 years equal to 0.45 g, which is in agreement with seismological estimates for the seismic risk in Santiago (Ordaz et al. 2014).

6.2 Structural and loss evaluation models

Linear structural model is assumed with lumped masses per floor having nominal values 1124 ton for ground level, 1805 ton for 2nd–5th story, 1753 ton for 6th–9th, 1675 ton for 10th story, 1616 ton for 11th–14th story, 1579 ton for 15th–18th story, 1527 ton for 19th story, 1158 ton for 20th story and 710 ton for 21th story. The stiffness matrix has been obtained by the design firm responsible for the project through the use of a commercial structural analysis software and has been subsequently structurally condensed to a planar model considering only one lateral displacement for each floor. This condensed stiffness matrix is then adjusted to take into account the effect of cracked concrete section and match the experimentally identified fundamental structural period which is 2.1 s (Zemp et al. 2011). The damping matrix is modeled through Rayleigh assumption by assigning an equal damping ratio for the first and second mode with a nominal value equal to 3 %. For this nominal model the first three modes (and participation factors in parenthesis) are 2.10 s (77 %), 0.54 s (16 %) and 0.25 s (5 %).

To examine the impact of structural uncertainties on the damper design two cases are examined for the structural model. The first case utilizes no uncertainties in the structural model, simply directly adopts the nominal values discussed above. This is referenced herein as nominal structure and denoted by abbreviation *NS*. The second case additionally considers uncertainty in the structural model description, particularly in the damping and stiffness matrices. This is referenced herein as probabilistic structure and denoted by abbreviation *PS*. For the uncertainty in the damping characteristics each damping ratio is modeled as Gaussian random variable with coefficient of variation 10 % and mean value the nominal one discussed above. For the uncertainty in the stiffness matrix a simplified characterization is adopted, understanding that the main dynamic property impacting the efficiency of mass dampers are the modal frequencies (since they are directly related to the tuning of the damper). Each modal frequency is treated as a Gaussian random variable with mean value the one resulting from the nominal structural model described above and coefficient of variation 10 %.

Table 1 Characteristics of fragility curves and expected repair cost for each story

Damage state	EDP	β_f	σ_f	n_{el}^b	Repair cost (\$/ n_{el})
Partitions					
1 (small cracks)	IDR ^a	0.21 %	0.60	350 m ²	22.30
2 (moderate cracks)	IDR	0.71 %	0.45	350 m ²	60.30
3 (severe damage)	IDR	1.2 %	0.45	350 m ²	92.70
Contents					
1 (damage)	PFA ^a	0.70 g	0.30	100	1000
Ceiling					
1 (some tiles fallen)	PFA	0.55 g	0.40	1500 m ²	15.20
2 (extensive tile fallout)	PFA	1.00 g	0.40	1500 m ²	120.10
3 (total ceiling collapse)	PFA	1.50 g	0.40	1500 m ²	237.70

^a IDR: peak interstory drift, PFA: peak floor acceleration

^b n_{el} number of elements per story

The characteristics for the loss assessment model are reported in Table 1; lognormal fragility functions are adopted with median β_f and standard deviation σ_f for three different damageable assemblies: partitions, ceiling and contents. For the first one the engineering demand parameter is taken as the peak inter-story drift and for the latter two as the peak floor acceleration. Note that damages to structural components are not included in this study since as discussed earlier are expected to have minimum contribution (behavior remains elastic even for stronger events). Variable n_e in Table 1 corresponds to the number of elements assumed per story whereas for each of the three different damageable assemblies different damage states are considered and the total repair cost per assembly is obtained by combining the contribution from all damage states. The fragility function parameters for the partitions and the suspended ceiling system are based on the recommendations in FEMA-P-58 (2012) whereas for the contents damageable subassembly the fragility curve used is similar to the one selected in Taflanidis and Beck (2009).

The discount rate is taken equal to 1.5 % and the lifetime t_{life} is assumed to be 50 years. The repair cost threshold is taken to correspond to probability $p_o = 10\%$ over t_{life} . The life-cycle cost and C_{thresh} for the uncontrolled structure (without the dampers) are, respectively, $\$2.11 \times 10^6$ and $\$1.22 \times 10^6$ for the probabilistic structure (PS) and $\$2.02 \times 10^6$ and $\$1.13 \times 10^6$ for the nominal structure (NS).

6.3 Damper cost

The upfront damper cost is approximated to be linearly related (Tse et al. 2012; Wang et al. 2015) to the damper mass $C_d(\mathbf{x}) = b_c m$ and three different cases are examined for this proportionality, $b_c = [1000 \ 1750 \ 2500]$ \$/ton. The higher upfront cost case is assumed to correspond to a TMD and is taken based on (Tse et al. 2012), additionally considering here that implementation is unidirectional and has no smart components (purely passive application). The other two, with lower installation cost, are representatives of a TLD-FR application. Since no detailed information is available for full-scale TLD-FR implementations these estimates are taken here to correspond to reduction of 30 or 60 % over the TMD case. This assumed reduction in the upfront cost is based on the argument, discussed in the introduction, for the lower installation/maintenance cost of liquid dampers over traditional TMDs.

6.4 Optimization details

The analysis is performed for three different efficiency indexes. The optimization is then established over the remaining design variables (r , α and ξ_m). The ranges assumed for developing the kriging metamodel (defining ultimately the admissible design space X) are $[0.2 \ 1.2]\%$ for r (it is assumed that greater than 1.2 % mass ratios are impractical to be achieved and ratios lower than 0.2 % are too small for practical implementation) $[1 \ 8]\%$ for ξ_m and $[0.94 \ 1]$ for α . The frequency ratio α is defined as the ratio between damper frequency and frequency corresponding to the fundamental mode of the nominal structural model (i.e. ignoring uncertainties in the model description). Due to the simplified assumption that the initial cost is related only to the total liquid mass (and not the exact tank geometry) incorporation of the efficiency index as a design variable was redundant since it is well-understood that a larger efficiency index would yield better results and therefore corresponds to the optimal design. $N = 10,000$ samples are used for the stochastic simulation and importance sampling densities q_{is} are formulated only for M and r_{rup} , which are expected to be the uncertain model parameters influencing more seismic

risk. The densities are chosen as truncated Gaussians in the range of each model parameter with mean and standard deviation of 7.3 and 1, respectively, for M and 70 and 70, respectively, for r_{rup} . These selections result in high accuracy estimation of the different risk characterizations with coefficient of variation below 3 % for all cases examined. The surrogate model to guide the optimization is established utilizing 1000 support points, following Latin hypercube sampling in X , whereas a blind-search approach is adopted for solving the multi-objective optimization problem. The accuracy of the developed surrogate model is first evaluated by calculating different error statistics using the leave-one-out cross-validation approach (Kohavi 1995). The accuracy established is ultimately high, with coefficient of determination over 97 % for most approximated response quantities and average error below 3 %. In addition, the accuracy of the estimated performance across the identified Pareto front is examined for some targeted cases. Similarly, good agreement is observed (less than 2 % error) for the estimated performance over the Pareto points.

6.5 Results and discussion

The discussion moves now to the results. Note that even though a complete Pareto-front is identified in each of the examined cases (meaning different values of γ and PS or NS characterization of the structure) in some of the figures a limited number of thirty representative designs are only used to describe each Pareto front in order to establish a more clear representation.

The Pareto front (representative points) for the PS (left column) and NS (right column) are shown in Fig. 5 for each of the three efficiency indexes considered (rows of each column) and the three cases for the upfront cost (curves within each column). Note that same scaling is used in all plots to facilitate a direct comparison. For the extreme designs (risk neutral and risk averse) the associated mass ratio r is shown as well as in parenthesis the decomposition of total cost to upfront (C_i/C) and repair cost (C_r/C). Then in Fig. 6 information about the optimal design configuration, i.e. optimal values of r , α and ξ_m , are reported for the case of efficiency index $\gamma = 0.7$ (results for other efficiency indexes follow identical trends), for r as a variation against the corresponding $C_{thresh}(\mathbf{x})$ value and for the other two as variation against r (reasons for this representation will be explained later). All Pareto-optimal configurations are shown (not just the representative ones from Fig. 5) whereas case presented corresponds to the intermediate cost assumption of 1750 \$/ton. Note, though, that all other cases for the upfront cost yield identical results; upfront cost does not impact the damper response and therefore has no influence on the optimal design configuration, only on the associated total cost $C(\mathbf{x})$ [it does not even influence $C_{thresh}(\mathbf{x})$]. Also in Fig. 6 the damper displacement threshold $y_{n,thresh}$ with probability of being exceeded 10 % over the considered 50 year lifetime is plotted [part (d) of the figure]. In this case results for all three considered efficiency indexes are reported. The calculation of threshold $y_{n,thresh}$ is performed in an identical manner as for $C_{thresh}(\mathbf{x})$, simply by using for each seismic event the respective response quantity (peak damper displacement) instead of the repair cost.

The results in Fig. 5 demonstrate that the addition of a mass damper can provide a considerable reduction for both $C(\mathbf{x})$ and $C_{thresh}(\mathbf{x})$ (compare these values to the ones reported earlier for the structure without the damper). The exact reduction for $C(\mathbf{x})$ depends, of course, on the characteristics for the upfront cost, which does not impact, though, $C_{thresh}(\mathbf{x})$ (the latter depends only on the damper efficiency). Larger values for the TLD-FR efficiency indexes yield, as expected, better life-cycle performance whereas reduction of the upfront cost for the damper also contributes to similar trends. This better performance

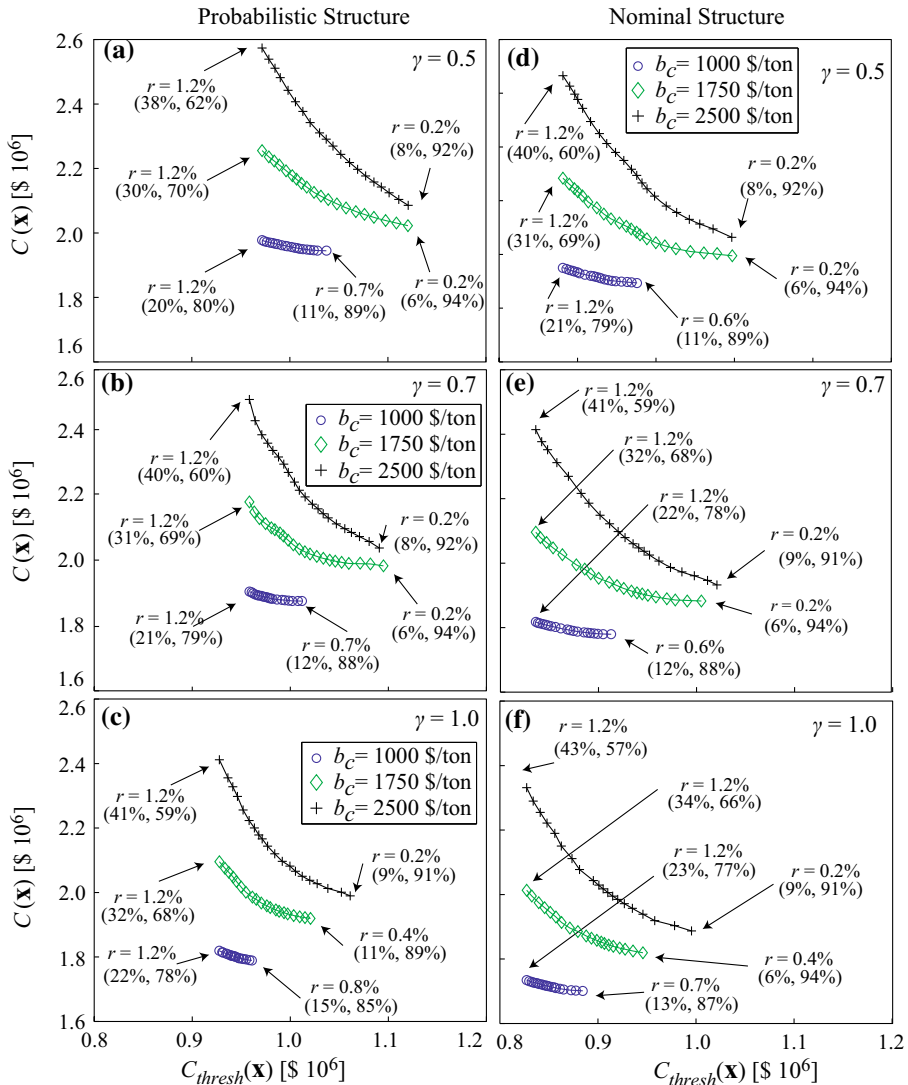


Fig. 5 Pareto front for different efficiency indexes (rows of each column) and different assumptions for upfront damper cost. Results for PS are presented in the *left column* and results for NS in the *right*. Also shown for the extreme designs are the corresponding mass ratio r and in parenthesis the decomposition of total cost to upfront cost and life-cycle repair cost (C_f/C , C_r/C)

is also associated with a reduction of the spread of the Pareto front. The dominant design variable along each Pareto front is the damper mass (see also discussion later) which is directly related to the damper protection efficiency as well its upfront cost. As one moves from risk-neutral towards risk-averse designs, the mass monotonically increases and ultimately hits the considered boundary (mass ratio of 1.2 %). Note that in some instances (low efficiency indexes or high upfront cost) even the risk-neutral design corresponds to the boundary of the admissible design space, i.e. the mass ratio corresponding to the

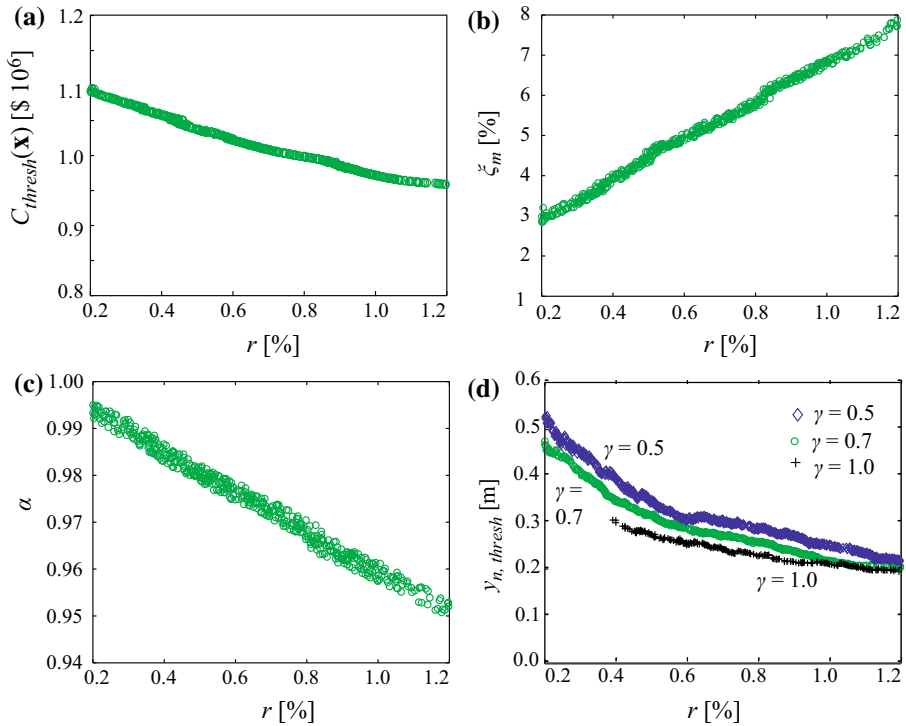


Fig. 6 Variation across the Pareto front of the optimal design configuration, mass ratio r (part **a**) damping ratio ζ_m (part **b**) and frequency ratio α (part **c**) as well the damper displacement (part **d**) with 10 % probability of being exceeded over the lifetime of 50 years $y_{n,thresh}$. Results correspond to PS, efficiency index 0.7 and upfront damper cost of 1750 \$/ton. For mass ratio r (part **a**) variation across the $C_{thresh}(x)$ value is reported whereas for all other cases variation with respect to r is reported. For the $y_{n,thresh}$ values for different efficiency indexes are also reported

smallest considered practical damper implementation for this case study. The stakeholder can ultimately make a choice among the different candidate solutions along the Pareto front by prioritizing the different competing objectives. This ultimately boils down to selection of the damper mass; larger masses yield greater reduction of C_{thresh} but a larger overall life-cycle cost (due to increase of upfront cost). Note that, especially for larger values of upfront cost b_c , moving towards risk-averse designs (smaller values for C_{thresh}) contributes to a significant increase in the total life cycle cost C .

Comparison between the PS and NS cases (columns of Fig. 5) shows similar behavior, with the former resulting in larger associated life-cycle cost and life-cycle losses threshold. This demonstrates that for the probabilistic structure detuning effects for the damper, stemming from the variability in the modal characteristics of the building, impact its efficiency. This is particularly evident for larger values of the efficiency index γ , which is something anticipated. For such larger values of γ the mass damper has greater potential impact against suppressing structural vibrations, so any detuning has a more profound effect on its performance. With respect to the cost decomposition across the Pareto front, for cases corresponding to larger values of the upfront cost the initial cost from installation of the dampers is a larger portion of the total life-cycle cost. This percentage increases as

risk-averse designs are prioritized (i.e. for smaller values of the C_{thresh} threshold), since these cases correspond to installation of larger dampers. Same pattern (larger percentage for the initial damper cost) also holds for higher values of the efficiency index; for dampers with the same mass and the same initial cost characteristics, larger efficiency indexes imply greater damper efficiency, leading to bigger reduction in earthquake losses and therefore to a more dominant contribution of the damper installation cost against the total life-cycle cost.

These results can be also utilized to facilitate the intended comparison between TMDs and TLDs-FR. TMDs correspond to $\gamma = 1$ and higher upfront cost ($b_c = 2500$ \$/ton for the cases examined here) whereas TLDs-FR to lower values of γ but also lower upfront cost, ($b_c = 1750$ \$/ton or 1000 \$/ton for the cases examined here, depending on what level of savings can be established). Figure 7 combines the results of interest from Fig. 5 to facilitate an easier comparison between these cases. As expected, for the same mass ratio TMDs offer greater protection efficiency, which translates ultimately to lower values of the threshold $C_{thresh}(\mathbf{x})$, though this might come at a higher overall cost due to the higher upfront damper cost. Whether this is the case depends on both the efficiency index established for the TLD-FR as well as the savings in the upfront cost. The lower upfront cost ($b_c = 1000$ \$/ton) yields always a superior life-cycle performance (Pareto front for it below the Pareto front corresponding to TMD); this means that same protection level can be accomplished at a lower overall cost. For the intermediate upfront cost case ($b_c = 1750$ \$/ton) the outcome depends on the efficiency index accomplished; for $\gamma = 0.5$ the TMD outperforms the TLD-FR whereas for $\gamma = 0.7$ the TLD-FR exhibits a slightly better performance. This discussion shows that TLDs-FR should be considered as an economically competitive option to TMDs for enhancement of seismic performance as long as proper design (avoidance of low efficiency indexes) can be accomplished. It also clearly demonstrates the importance of the proposed framework for (1) establishing a comparison of different type of dampers based on life-cycle cost concepts and (2) explicitly addressing the upfront cost of the dampers in the analysis. Should be stressed that these outcomes

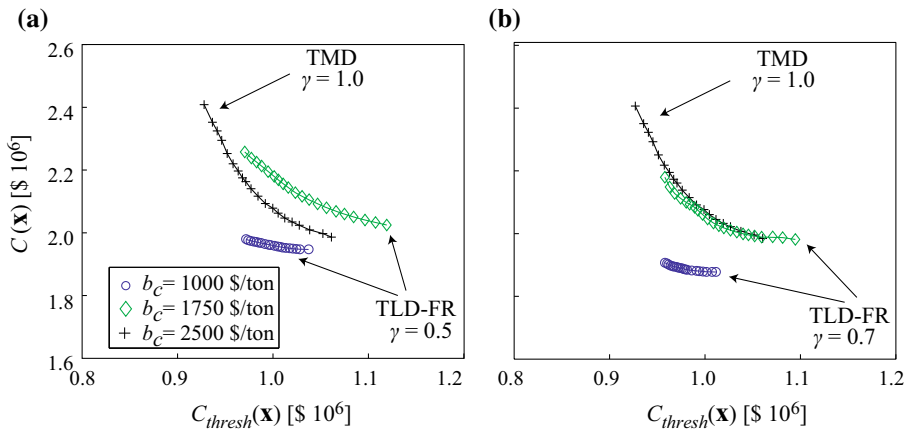


Fig. 7 Comparison of performance (in terms of corresponding Pareto fronts) of TMD ($\gamma = 1$ and high upfront cost) and TLD-FR with efficiency index either $\gamma = 0.7$ (part a) or $\gamma = 0.5$ (part b). For the TLD-FR two cases for upfront cost are presented corresponding to savings of 30 or 60 % respectively over the TMD implementation. **a** Comparison of TMD to TLD-FR with $\gamma = 0.5$. **b** Comparison of TMD to TLD-FR with $\gamma = 0.7$

depend on the exact cost characteristics of the case study examined, and warrant a different socio-economic evaluation in each implementation of interest, as well a more detailed evaluation of the upfront cost for TLDs-FR.

Moving, now, to the optimal design characteristics (Fig. 6), the main design variable distinguishing the behavior across the Pareto front is the mass ratio as each mass ratio is uniquely associated with a performance level [level of protection and therefore $C_{thresh}(\mathbf{x})$ value]. This is expected as discussed earlier since this is the characteristic that directly impacts both the upfront cost as well as the damper efficiency. This is the reason the trends for the remaining design variables are reported as variation with respect to the mass ratio. The frequency and damping ratios simply take proper tuning values for the respective mass ratio and efficiency index (Chang 1999), showing further some variability along a nominal trend. This observed variability stems from the fact that values for the frequency and damping ratio close to the optimal yield very similar efficiency, whereas these values do not impact the upfront cost. This leads to similar performance in the objective space for a range of near-optimal values. With respect to the damper displacement, an important issue when considering space-constraints for placement of the damper, larger mass ratios or efficiency indexes result to lower demands, a characteristic well anticipated (Chang 1999). Of course the impact of these demands depends really on the characteristic of the case examined (architectural constraints) whereas one needs to additionally consider that these displacements represent fundamentally different responses for each type of mass damper. For TLDs-FR they are related to maximum vertical displacements of the roof, which should be considered easier to accommodate compared to the horizontal displacement of TMDs.

Based on the desired Pareto optimal solution and the associated optimal parametric configuration the designer can finally select the tank configuration using the mapping between the parametric space and the real geometry space discussed in Sect. 3. For example, if the risk-neutral is chosen for the PS and the upfront cost case $b_c = 1000$ \$/ton, then the optimal parametric configurations for $\gamma = 0.5$ is $r = 0.2$ %, $\omega_m = 2.98$ rad/s (corresponding to $\alpha = 0.996$) and $\zeta_m = 3.34$ %. For a rectangular tank (as the one shown in Fig. 1b) these correspond to tank length $L = 3.18$ m, liquid height $H = 1.55$ m and width 13.46 m. The optimal damping ratio ζ_m can be then used to select the external damper properties. Note that the desired width can be satisfied by using multiple tanks that better fit any architectural constraints. If this geometric configuration is impractical based on available space, then one can examine different tank geometries that can offer greater versatility in selecting the tank characteristics (Ruiz et al. 2015c).

Finally, the effect of neglecting structural uncertainties is examined in Fig. 8. This figure shows the performance established for the probabilistic structure (PS) for the respective Pareto front (best performance that can be accomplished) as well as the design corresponding to the optimal solution from the nominal structure (NS). The comparison answers the question; what would have been the performance degradation if structural uncertainties were neglected at the design stage (utilize design from NS) but really existed (evaluate performance for the PS and compare to the respective Pareto front)? The results show that the explicit consideration of uncertainties does improve the robustness of the performance (Pareto curves are indeed different) with the effect being greater (larger discrepancies between the curves) when the efficiency of the damper is greater (meaning larger values of the efficiency index or smaller values for the C_{thresh} which, recall, corresponds to larger mass ratios). This result stresses the importance of a design framework that can explicitly incorporate uncertainties related to the structural characteristics within the problem formulation. The simulation-based approach discussed here can seamlessly

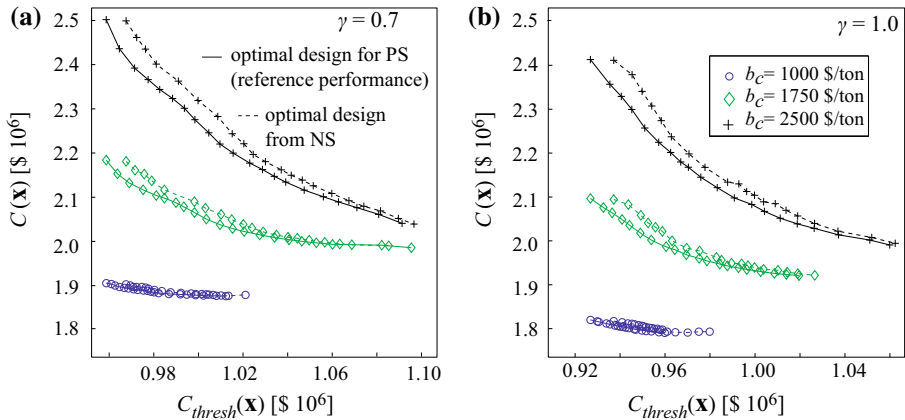


Fig. 8 Impact of neglecting structural uncertainties in the design stage. Performance (in terms of Pareto front) for efficiency indexes $\gamma = 0.7$ (part **a**) and $\gamma = 1$ (part **b**) and different assumptions for upfront damper cost for the PS are shown. Pareto front from this design case (representing the reference performance) as well as performance for the optimal solution corresponding to the nominal structure (NS) are shown

facilitate this goal since it poses no constraints on the complexity of the probability and numerical models that are utilized.

7 Conclusions

The life-cycle based assessment/design of TLDs-FR (or more generally mass dampers) was discussed in this paper considering a risk characterizations appropriate for the Chilean region. It was first demonstrated that considering the unique characteristics of the regional hazard (long duration excitations without directivity-pulse components) mass dampers offer an efficient seismic protection option even for reducing transient response characteristics (peak response quantities). Afterwards, a multi-objective optimization problem was formulated considering as design criteria the total life-cycle cost and consequences (repair cost) for low-likelihood events. A simulation-based, probabilistic framework was adopted for quantifying/assessing these criteria. Within this framework structural performance is described through time-history analysis, adopting a comprehensive, assembly-based vulnerability approach to quantify seismic losses in a detailed, component level. To characterize the seismic hazard a stochastic ground motion models was calibrated to provide predictions that are compatible with ground motion prediction equations (attenuation relationships) that have been recently proposed for Chile. For performing the design optimization a surrogate modeling formulation was adopted, which further supports a highly efficient design for different assumptions for the upfront damper cost. The overall framework allows for adoption of complex numerical and probability models, facilitating a comprehensive hazard characterization. In addition, it allows for explicitly considering all important sources of uncertainty in the model description. For mass dampers applications this means that uncertainties related to the dynamic characteristics of the primary structure can be easily incorporated in the design problem formulation.

Exploiting these features the life-cycle based assessment/design of mass dampers for a 21-story structure was examined in the case-study. The multi-objective formulation provided in the context of this example a range of Pareto optimal solutions, allowing the building stakeholder to make the final choice prioritizing between the two competing objectives; reduction of the total cost or improved protection against low likelihood but high impact seismic events. Additionally, by considering different upfront damper cost, a comparison between TMDs and TLDs-FR was established. Even though TMDs offer enhanced performance for the same mass ratio, when considering the higher upfront cost for them it was demonstrated that TLDs-FR ultimately have the potential to outperform them (at least in the context of this case study); for the same life-cycle cost their application corresponds to better overall protection. Therefore TLDs-FR should be considered as an economically competitive option to TMDs for enhancement of seismic performance as long as proper design (avoidance of low efficiency indexes for them) can be accomplished. In addition, explicitly considering uncertainties related to structural dynamic characteristics was shown to provide enhanced robustness in the damper implementation.

Acknowledgments Financial support was provided by the Pontificia Universidad Católica de Chile, by the University of Notre Dame and by the National Research Center for Integrated Natural Disaster Management CONICYT/FONDAP/15110017 (Chile). This support is gratefully acknowledged. The dynamic properties of the structure considered in the case study described in Sect. 6 were provided by VMB Ingeniería Estructural (Santiago, Chile).

Appendix A: Parametric formulation for the equations of motion for the TLD-FR

The numerical model for the TLD-FR has two components (Ruiz et al. 2015b). The first component corresponds to the motion of the liquid and is described through a finite element formulation that condenses the vibratory response to the motion of the liquid-surface (Ruiz et al. 2015a), an idea first presented in (Almazan et al. 2007). The second component corresponds to the vibration of the roof and is similarly described through finite element principles, adopting a coincidental mess with the one used to describe the motion of the liquid-surface. The effect of external dampers is also incorporated in this second component. The two components are ultimately combined through the pressures created at the common interface (liquid surface) to provide the final coupled numerical model (Ruiz et al. 2015b).

$$\mathbf{M}_a \ddot{\boldsymbol{\eta}}_s + \mathbf{C}_a \dot{\boldsymbol{\eta}}_s + \mathbf{K}_a \boldsymbol{\eta}_s = -\mathbf{R}_a \ddot{u}_b \quad (10)$$

where vector $\boldsymbol{\eta}_s$ contains the vertical nodal displacements at the free surface, \ddot{u}_b is the acceleration at the base of the tank, matrices \mathbf{M}_a , \mathbf{C}_a , \mathbf{K}_a are “equivalent” mass, damping and stiffness matrices and vector \mathbf{R}_a is conceptually similar to an influence coefficient vector. Full derivation of these matrices is included in (Ruiz et al. 2015b). The transmitted force F at the base of the tank is:

$$F = -\rho d \mathbf{A} \ddot{\boldsymbol{\eta}}_s - \rho d B \ddot{u}_b \quad (11)$$

where ρ is the liquid density, d is the tank width, \mathbf{A} is a row vector and B a scalar variable both obtained through the aforementioned numerical formulation.

The parametric formulation is then established through modal reduction, keeping only the first mode of the TLD-FR (the mode that is tuned to the vibration of the structure). Let

Φ denote the eigenvector for the eigenvalue problem corresponding to mass and stiffness matrices \mathbf{M}_a and \mathbf{K}_a . Then (10) is transformed into:

$$M_m \ddot{y} + C_m \dot{y} + K_m y = -R_m \ddot{u}_b \tag{12}$$

where

$$M_m = \Phi^T \mathbf{M}_a \Phi; \quad C_m = \Phi^T \mathbf{C}_a \Phi; \quad K_m = \Phi^T \mathbf{K}_a \Phi; \quad R_m = \Phi^T \mathbf{R}_a; \quad \eta_s = \Phi y \tag{13}$$

The modal coordinate y can be further normalized as $y_n = y M_m / R_m$, and by defining the natural frequency in the fundamental sloshing mode as $\omega_m = \sqrt{K_m / M_m}$ and the damping ratio as $\zeta_m = C_m / 2 M_m \omega_m$, (12) yields (1). It is evident through this formulation that $2\zeta_m \omega_m \dot{y}_n$ and $\omega_m^2 y_n$ can be treated as damping and spring forces, respectively, for the mass damper.

The expression for the transmitted force (11) also simplifies to

$$F = -\rho d \left[\mathbf{A} \Phi \frac{R_m}{M_m} \right] \ddot{y}_n - \rho d B \ddot{u}_b \tag{14}$$

and setting as $m = \rho d B$ the liquid mass and as $\gamma = \mathbf{A} \Phi (R_m / B M_m)$ the efficiency index yields ultimately (2). Note that term γm can be equivalently considered as the convective mass, i.e. the portion of the mass that has a dynamic contribution to the liquid vibration.

Appendix B: Details on stochastic ground motion model

According to the adopted stochastic ground motion model, the discretized time series of the ground motion, $\ddot{a}_g(t)$, is expressed as

$$\ddot{a}_g(t) = e(t, \theta_g) \left\{ \sum_{i=1}^k \frac{h[t - t_i, \theta_g(t_i)]}{\sqrt{\sum_{j=1}^k h[t - t_j, \theta_g(t_j)]^2}} w_w(i\Delta t) \right\} k\Delta t < t < (k + 1)\Delta t \tag{15}$$

where $[w_w(i\Delta t): i = 1, 2, \dots, N_T]$ is a white noise sequence, $\Delta t = 0.005$ s is the chosen discretization interval, $e(t, \theta_g)$ is the time-modulating function, and $h[t - \tau, \theta_g(\tau)]$ is an impulse response function corresponding to the pseudo-acceleration response of a single-degree-of-freedom (SDOF) linear oscillator with time varying frequency $\omega_f(\tau)$ and damping ratio $\zeta_f(\tau)$, in which τ denotes the time of the pulse

$$\begin{aligned} h[t - \tau, \theta_g(\tau)] &= \frac{\omega_f(\tau)}{\sqrt{1 - \zeta_f^2(\tau)}} \exp[-\omega_f(\tau)\zeta_f(\tau)(t - \tau)] \sin \left[\omega_f(\tau)\sqrt{1 - \zeta_f^2(\tau)}(t - \tau) \right]; \quad \tau \leq t \\ &= 0; \text{ otherwise} \end{aligned} \tag{16}$$

The time varying characteristics are

$$\omega_f(\tau) = \omega_r + (\omega_p - \omega_r) \left(\frac{\omega_s - \omega_r}{\omega_p - \omega_r} \right)^{\tau/t_{max}} \tag{17}$$

$$\zeta_f(\tau) = \alpha_f(\tau)/\omega_f(\tau) \quad \text{where } \alpha_f(\tau) = \omega_p \zeta_p + (\omega_r \zeta_r - \omega_p \zeta_p) \tau/t_r$$

with ω_p (primary wave frequency), ω_s (secondary wave frequency), ω_r (surface wave frequency), ζ_p (primary wave damping), and ζ_r (surface wave damping) ultimately corresponding to the primary model parameters for the filter, t_{max} corresponding to the time at which maximum intensity of the ground motion is achieved and $t_r = \alpha_{dur} t_{95}$ corresponding to a sufficiently large time, chosen to be proportional to the time that 95 % of the Arias intensity is reached, denoted t_{95} .

The time envelope $e(t, \theta_g)$ is parameterized by

$$e(t, \theta_g) = e(t, I_a, \alpha_2, \alpha_3) = \sqrt{I_a} \left[\sqrt{\frac{2 (2\alpha_3)^{2\alpha_2-1}}{\pi \Gamma(2\alpha_2 - 1)}} \right] t^{\alpha_2-1} \exp(-\alpha_3 t) \tag{18}$$

where $\Gamma(\cdot)$ is the gamma function, I_a is the Arias intensity expressed in terms of g , and $\{\alpha_2, \alpha_3\}$ are additional parameters controlling the shape and total duration of the envelope that can be related to the strong motion duration, D_{5-95} (defined as the duration for the Arias intensity to increase from 5 to 95 % of its final value), and the peak of the envelope function, λ_p . The latter is defined as the ratio of time corresponding to the peak of the envelope to the time corresponding to 95 % of its peak value. The pair $\{\alpha_2, \alpha_3\}$ can be easily determined based on the values of $\{D_{5-95}, \lambda_p\}$ (Vetter et al. 2015).

Ultimately, the ground motion model has as parameters $\theta_g = \{I_a, D_{5-95}, \lambda_p, \alpha_{dur}, \omega_p, \omega_s, \omega_r, \zeta_p, \zeta_r\}$ and the functional form for their predictive relationships are chosen as

Table 2 Optimized coefficients (Coef.) for the predictive relationships of the stochastic ground motion model parameters to achieve GMPE compatibility

Coef	Value	Coef	Value	Coef	Value	Coef	Value	Coef	Value
$c_{1,1}$	-17.6734	$c_{1,8}$	0.427	$c_{3,3}$	-0.0464	$c_{6,1}$	3.1995	$c_{8,1}$	-3.6364
$c_{1,2}$	4.2932	$c_{2,1}$	0.7694	$c_{4,1}$	-0.2706	$c_{6,2}$	-0.0339	$c_{8,2}$	0.211
$c_{1,3}$	-0.0895	$c_{2,2}$	0.5626	$c_{4,2}$	0.0071	$c_{6,3}$	-0.0336	$c_{8,3}$	-0.0195
$c_{1,4}$	0.0068	$c_{2,3}$	-0.3978	$c_{4,3}$	0.027	$c_{7,1}$	2.3025	$c_{9,1}$	-1.8895
$c_{1,5}$	-0.1565	$c_{2,4}$	5.0729	$c_{5,1}$	3.7109	$c_{7,2}$	-0.3227	$c_{9,2}$	0.0904
$c_{1,6}$	0.0001	$c_{3,1}$	-1.122	$c_{5,2}$	-0.0079	$c_{7,3}$	-0.0345	$c_{9,3}$	-0.0175
$c_{1,7}$	-2.7709	$c_{3,2}$	-0.043	$c_{5,3}$	-0.0119				

$$\begin{aligned}
\ln(I_a) &= c_{1,1} + c_{1,2}M + c_{1,3}r_{rup} + c_{1,4}r_{rup}M + c_{1,5}M^2 + c_{1,6}r_{rup}^2 + c_{1,7} \ln(M) + c_{1,8} \ln(r_{rup}); \\
\ln(D_{5-95}) &= c_{2,1} + c_{2,2}M + c_{2,3} \ln\left(\sqrt{r_{rup}^2 + c_{2,4}^2}\right); \ln(\lambda_p) = c_{3,1} + c_{3,2}M + c_{3,3}r_{rup}; \\
\ln(\alpha_{dur}) &= c_{4,1} + c_{4,2}M + c_{4,3}r_{rup}; \\
\ln(\omega_p/2\pi) &= c_{5,1} + c_{5,2}M + c_{5,3}r_{rup}; \ln(\omega_s/2\pi) = c_{6,1} + c_{6,2}M + c_{6,3}r_{rup}; \\
\ln(\omega_r/2\pi) &= c_{7,1} + c_{7,2}M + c_{7,3}r_{rup}; \\
\ln(\zeta_p) &= c_{8,1} + c_{8,2}M + c_{8,3}r_{rup}; \ln(\zeta_r) = c_{9,1} + c_{9,2}M + c_{9,3}r_{rup}
\end{aligned} \tag{19}$$

with the coefficients $c_{i,l}$ $i = 1, \dots, 9$, $l = 1, \dots, 8$ formulating the (regression) coefficient vector \mathbf{c} , representing ultimately the vector optimized to establish the desired hazard compatibility. For the model tuning discussed in Sect. 5 (with results also presented in Fig. 4) the optimized coefficients are shown in Table 2.

References

- Almazan JL, Cerda FA, De la Liera JC, Lopez-Garcia D (2007) Linear isolation of stainless steel legged thin-walled tanks. *Eng Struct* 29(7):1596–1611
- Ang H-SA, Lee J-C (2001) Cost optimal design of R/C buildings. *Reliab Eng Syst Saf* 73:233–238
- Balendra T, Wang CM, Rakesh G (1999) Vibration control of various types of buildings using TLCD. *J Wind Eng Ind Aerodyn* 83(1):197–208
- Boroschek R, Contreras V (2012) Strong ground motion from the 2010 Mw 8.8 Maule Chile earthquake and attenuation relations for Chilean subduction zone interface earthquakes. In: Proceedings of the international symposium on engineering lessons learned from the 2011 Great East Japan earthquake, Tokyo, Japan.
- Bozorgnia Y, Bertero V (2004) *Earthquake Engineering: From Engineering Seismology to Performance-based Engineering*. CRC Press, Boca Raton
- Bray JD, Rodriguez-Marek A (2004) Characterization of forward-directivity ground motions in the near-fault region. *Soil Dyn Earthq Eng* 24:815–828
- Cha EJ, Ellingwood BR (2012) Risk-averse decision-making for civil infrastructure exposed to low-probability, high-consequence events. *Reliab Eng Syst Saf* 104:27–35
- Chakraborty S, Roy BK (2011) Reliability based optimum design of tuned mass damper in seismic vibration control of structures with bounded uncertain parameters. *Probab Eng Mech* 26(2):215–221
- Chang CC (1999) Mass dampers and their optimal designs for building vibration control. *Eng Struct* 21:454–463
- Coello CAC, Van Veldhuizen DA, Lamont GB (2002) *Evolutionary algorithms for solving multi-objective problems*, vol 242. Springer, New York
- Daniel Y, Lavan O (2014) Gradient based optimal seismic retrofitting of 3D irregular buildings using multiple tuned mass dampers. *Comput Struct* 139:84–97
- De Angelis M, Perno S, Reggio A (2012) Dynamic response and optimal design of structures with large mass ratio TMD. *Earthq Eng Struct Dyn* 41(1):41–60
- De la Llera JC, Lüders C, Leigh P, Sady H (2004) Analysis, testing, and implementation of seismic isolation of buildings in Chile. *Earthq Eng Struct Dyn* 33(5):543–574
- Debbarma R, Chakraborty S, Ghosh S (2010) Unconditional reliability-based design of tuned liquid column dampers under stochastic earthquake load considering system parameters uncertainties. *J Earthq Eng* 14(7):970–988
- Den Hartog JP (1947) *Mechanical vibrations*. McGraw-Hill Inc, New York
- EERI Special Earthquake Report (2010) Learning from earthquakes: the Mw 8.8 Chile earthquake of February 27, 2010. *Earthq Eng Res Inst Newsl* 44(6)
- FEMA-P-58 (2012) *Seismic performance assessment of buildings*. American Technology Council, Redwood City
- Fragiadakis M, Lagaros ND, Papadrakakis M (2006) Performance-based multiobjective optimum design of steel structures considering life-cycle cost. *Struct Multidiscip Optim* 32:1–11

- Fujino Y, Sun L, Pacheco BM, Chaiseri P (1992) Tuned liquid damper (TLD) for suppressing horizontal motion of structures. *J Eng Mech* 118(10):2017–2030
- Gidaris I, Taflanidis AA (2015) Performance assessment and optimization of fluid viscous dampers through life-cycle cost criteria and comparison to alternative design approaches. *Bull Earthq Eng* 13(4):1003–1028
- Gidaris I, Taflanidis AA, Mavroeidis GP (2014) Multi-objective design of fluid viscous dampers using life-cycle cost criteria. In: 10th national conference in earthquake engineering, Anchorage.
- Goulet CA, Haselton CB, Mitrani-Reiser J, Beck JL, Deierlein G, Porter KA, Stewart JP (2007) Evaluation of the seismic performance of code-conforming reinforced-concrete frame building-From seismic hazard to collapse safety and economic losses. *Earthq Eng Struct Dyn* 36(13):1973–1997
- Hitchcock PA, Kwok KCS, Watkins RD, Samali B (1997) Characteristics of liquid column mass dampers (LCVA)-II. *Eng Struct* 19(2):135–144
- Hoang N, Fujino Y, Warnitchai P (2008) Optimal tuned mass damper for seismic applications and practical design formulas. *Eng Struct* 30(3):707–715
- Housner GW (1957) Dynamic pressures on accelerated fluid containers. *Bull Seismol Soc Am* 47(1):15–35
- Jalayer F, Beck JL (2008) Effects of two alternative representations of ground-motion uncertainty in probabilistic seismic demand assessment of structures. *Earthq Eng Struct Dyn* 37(1):61–79
- Kaneko S, Mizota Y (2000) Dynamical modeling of deepwater-type cylindrical tuned liquid damper with a submerged net. *J Press Vessel Technol* 122(1):96–104
- Kareem A (1990) Reduction of wind induced motion utilizing a tuned sloshing damper. *J Wind Eng Ind Aerodyn* 36:725–737
- Kohavi R (1995) A study of cross-validation and bootstrap for accuracy estimation and model selection. In: Proceedings of the international joint conference on artificial intelligence, pp 1137–1145
- Lee CS, Goda K, Hong HP (2012) Effectiveness of using tuned-mass dampers in reducing seismic risk. *Struct Infrastruct Eng* 8(2):141–156
- Leyton F, Ruiz S, Sepúlveda SA (2009) Preliminary re-evaluation of probabilistic seismic hazard assessment in Chile: from Arica to Taitao Peninsula. *Adv Geosci* 22(22):147–153
- Lin C-C, Chen C-L, Wang J-F (2010) Vibration control of structures with initially accelerated passive tuned mass dampers under near-fault earthquake excitation. *Comput Aided Civil Infrastruct Eng* 25(1):69–75
- Love JS, Tait MJ (2010) Nonlinear simulation of a tuned liquid damper with damping screens using a modal expansion technique. *J Fluids Struct* 26(7):1058–1077
- Marano GC, Greco R, Trentadue F, Chiaia B (2007) Constrained reliability-based optimization of linear tuned mass dampers for seismic control. *Int J Solids Struct* 44(22–23):7370–7388
- Marian L, Giaralis A (2014) Optimal design of a novel tuned mass-damper-inertor (TMDI) passive vibration control configuration for stochastically support-excited structural systems. *Probab Eng Mech* 38:156–164
- Marler RT, Arora JS (2004) Survey of multi-objective optimization methods for engineering. *Struct Multidiscip Optim* 26:369–395
- Matta E (2011) Performance of tuned mass dampers against near-field earthquakes. *Struct Eng Mech* 39(5):621–642
- Matta E, De Stefano A (2009) Seismic performance of pendulum and translational roof-garden TMDs. *Mech Syst Signal Process* 23(3):908–921
- Matta E, De Stefano A, Spencer BF (2009) A new passive rolling pendulum-vibration absorber using a non-axial-symmetrical guide to achieve bidirectional tuning. *Earthq Eng Struct Dyn* 38(15):1729–1750
- Mavroeidis GP, Dong G, Papageorgiou AS (2004) Near-fault ground motions, and the response of elastic and inelastic single-degree-of-freedom (SDOF) systems. *Earthq Eng Struct Dyn* 33(9):1023–1049
- Moroni MO, Sarrazin M, Herrera R (2011) Research activities in Chile on base isolation and passive energy dissipation. In: Proceedings of the 12th world conference on seismic isolation, energy dissipation and active vibration control of structures, Sochi.
- Ordaz MG, Cardona O-D, Salgado-Gálvez MA, Bernal-Granados GA, Singh SK, Zuloaga-Romero D (2014) Probabilistic seismic hazard assessment at global level. *Int J Disaster Risk Reduct* 10:419–427
- Papadimitriou K (1990) Stochastic characterization of strong ground motion and application to structural response. Report No. EERL 90-03, California Institute of Technology, Pasadena.
- Porter KA, Kiremidjian AS, LeGrue JS (2001) Assembly-based vulnerability of buildings and its use in performance evaluation. *Earthq Spectra* 18(2):291–312
- Porter KA, Kennedy RP, Bachman RE (2007) Creating fragility functions for performance-based earthquake engineering. *Earthq Spectra* 23(2):471–489
- Power M, Chiou B, Abrahamson N, Bozorgnia Y, Shantz T, Roblee C (2008) An overview of the NGA project. *Earthq Spectra* 24(1):3–21

- Rezaeian S, Der Kiureghian A (2010) Simulation of synthetic ground motions for specified earthquake and site characteristics. *Earthq Eng Struct Dyn* 39(10):1155–1180
- Ruiz RO (2015) A new type of tuned liquid damper and its effectiveness in enhancing seismic performance; numerical characterization, experimental validation, parametric analysis and life-cycle based design. Pontificia Universidad Católica de Chile, Santiago
- Ruiz RO, Lopez-García D, Taflanidis AA (2015a) An efficient computational procedure for the dynamic analysis of liquid storage tanks. *Eng Struct* 85:206–218
- Ruiz RO, Lopez-García D, Taflanidis AA (2015b) Modeling and experimental validation of a new type of tuned liquid damper *Acta Mechan.* doi:[10.1007/s00707-015-1536-7](https://doi.org/10.1007/s00707-015-1536-7)
- Ruiz RO, Lopez-García D, Taflanidis AA (2015c) Tuned liquid damper with floating roof: A new device to control earthquake-induced vibrations in structures. In: XI Congreso Chileno de Sismología e Ingeniería Sísmica, Santiago.
- Sakai F, Takaeda S, Tamaki T (1989) Tuned liquid column damper-new type device for suppression of building vibrations. In: Proceedings of the international conference of high-rise buildings, Nanjing, pp 926–931
- Salvi J, Rizzi E, Gavazzeni M (2014) Analysis on the optimum performance of tuned mass damper devices in the context of earthquake engineering. In: EURO DYN 2014-IX international conference on structural dynamics, Porto, Portugal, 30 June–2 July. Universidade do Porto, Faculdade de Engenharia, FEUP, pp 1729–1736
- Scherbaum F, Cotton F, Staedtke H (2006) The estimation of minimum-misfit stochastic models from empirical ground-motion prediction equations. *Bull Seismol Soc Am* 96(2):427–445
- Shin H, Singh MP (2014) Minimum failure cost-based energy dissipation system designs for buildings in three seismic regions Part II: Application to viscous dampers. *Eng Struct* 74:275–282
- Soto MG, Adeli H (2013) Tuned mass dampers. *Arch Comput Methods Eng* 20(4):419–431
- Spall JC (2003) Introduction to stochastic search and optimization. Wiley-Interscience, New York
- Taflanidis AA, Beck JL (2009) Life-cycle cost optimal design of passive dissipative devices. *Struct Saf* 31(6):508–522
- Taflanidis AA, Beck JL, Angelides DA (2007) Robust reliability-based design of liquid column mass dampers under earthquake excitation using an analytical reliability approximation. *Eng Struct* 29(12):3525–3537
- Tait MJ, Isyumov N, El Damatty AA (2007) Effectiveness of a 2D TLD and its numerical modeling. *J Struct Eng* 133(2):251–263
- Tributsch A, Adam C (2012) Evaluation and analytical approximation of tuned mass damper performance in an earthquake environment. *Smart Struct Syst* 10(2):155–179
- Tse KT, Kwok KCS, Tamura Y (2012) Performance and cost evaluation of a smart tuned mass damper for suppressing wind-induced lateral-torsional motion of tall structures. *J Struct Eng* 138(4):514–525
- Vamvatsikos D, Cornell CA (2005) Direct estimation of seismic demand and capacity of multidegree-of-freedom systems through incremental dynamic analysis of single degree of freedom approximation 1. *J Struct Eng* 131(4):589–599
- Vetter CR, Taflanidis AA, Mavroeidis GP (2015) Tuning of stochastic ground motion models for compatibility with ground motion prediction equations. *Earthq Eng Struct Dyn.* doi:[10.1002/eqe.2690](https://doi.org/10.1002/eqe.2690)
- Wang D, Tse TKT, Zhou Y, Li Q (2015) Structural performance and cost analysis of wind-induced vibration control schemes for a real super-tall building. *Struct Infrastruct Eng* 11(8):990–1011
- Wong KK (2008) Seismic energy dissipation of inelastic structures with tuned mass dampers. *J Eng Mech*
- Zemp R, de la Llera JC, Roschke P (2011) Tall building vibration control using a TM-MR damper assembly: Experimental results and implementation. *Earthq Eng Struct Dyn* 40(3):257–271